

Tetrahedral hydrocarbon nanoparticles in space: X-ray spectra

G. Bilalbegović¹, A. Maksimović², L. A. Valencic^{3,4}

¹Department of Physics, Faculty of Science, University of Zagreb, Bijenička cesta 32, 10000 Zagreb, Croatia

²Center of Excellence for Advanced Materials and Sensing Devices, Rudjer Bošković Institute, Bijenička cesta 54, 10000 Zagreb, Croatia

³NASA Goddard Space Flight Center, Greenbelt, MD 20771, USA

⁴The Johns Hopkins University, Department of Physics & Astronomy, 366 Bloomberg Center, 3400 N. Charles St., Baltimore, MD 21218, USA

15 October 2018

ABSTRACT

It has been proposed, or confirmed, that diamond nanoparticles exist in various environments in space: close to active galactic nuclei, in the vicinity of supernovae and pulsars, in the interior of several planets in the Solar system, in carbon planets and other exoplanets, carbon-rich stars, meteorites, in X-ray active Herbig Ae/Be stars, and in the interstellar medium. Using density functional theory methods we calculate the carbon K-edge X-ray absorption spectrum of two large tetrahedral nanodiamonds: $C_{26}H_{32}$ and $C_{51}H_{52}$. We also study and test our methods on the astrophysical molecule CH_4 , the smallest C-H tetrahedral structure. A possible detection of nanodiamonds from X-ray spectra by future telescopes, such as the project *Arcus*, is proposed. Simulated spectra of the diffuse interstellar medium using Cyg X-2 as a source show that nanodiamonds studied in this work can be detected by *Arcus*, a high resolution X-ray spectrometer mission selected by NASA for a Phase A concept study.

Key words: astrochemistry – ISM: molecules – methods: numerical – X-rays: individuals: V892 Tau, HD 97048, Cyg X-2 – X-rays: ISM – galaxies: active

1 INTRODUCTION

Nanoparticles of diamonds (also known as nanodiamonds, diamondoids, diamondoid molecules, diamond clusters) are structures important in various branches of science (Galli 2010; Clay et al. 2015). Saslaw & Gaustad (1969) suggested a long time ago that diamond structures could play an important role in astrophysical phenomena. An earlier work about diamonds in the astrophysical context exists (Wentorf & Bovenkerk 1961). The authors compared “the diamonds of men and the diamonds of nature” to shed light on their formation. However, the question of how diamonds form in space is still not completely solved.

1.1 Meteorites and rocks on Earth

Nanodiamonds were found at several locations in the Younger Dryas boundary sediments (Kennett et al. 2009). It was proposed that these nanoparticles formed during impacts of comets or asteroids. Nanoparticles of diamonds are the most abundant form of carbon in carbonaceous chondrite meteorites (Lewis et al. 1987; Lewis, Anders & Draine 1989). It is accepted today that these meteoritic nanodiamonds were formed in the Solar system by processes similar to chemical vapor deposition (Daulton et al. 1996; Dai et al. 2002).

1.2 Supernovae, the interstellar medium, pulsars, carbon planets and stars

It was proposed that diamond nanoparticles form in dust processing by strong shock waves in the vicinity of a supernovae (Tielens et al. 1987). Tielens et al. (1987) calculated that approximately 5% of the carbon in the ISM exists in the form of (5-100) Å nanodiamonds.

Nanodiamonds were suggested as carriers of extended red emission (Duley 1988; Chang, Chen & Kwok 2006). Rai & Rastogi (2012) found that nanodiamonds are good candidates for a source of the observed extinction along anomalous sightlines.

It was estimated that the binary object of the pulsar J1719-1438 has the minimum density of 23 g/cm^3 (Bailes et al. 2011). The chemical composition, dimensions, and pressures of J1719-1438 b indicate that it consists of diamonds. Kuchner & Seager (2005) proposed the existence of such carbon planets that contain more carbon than oxygen and suggested that substantial amount of diamond should exist there. The carbon-rich composition and the existence of diamonds has been predicted for the pulsar planets (Margalit & Metzger 2017). Helling et al. (2017) presented a kinetic model of cloud formation around carbon-rich exoplanets and brown dwarfs. They found that inner parts of carbon-rich clouds could be made of diamonds. It was also proposed that diamonds form in the envelopes of carbon-rich stars, such as HR 4049 that is at the post-AGB phase of evolution (Geballe et al. 1989; Van Kerckhoven, Tielens & Waelkens 2002).

1.3 Active galactic nuclei

A dust model consisting of nanodiamonds was one of approaches used to explain the big blue bump in the spectral energy distribution of active galactic nuclei (AGNs) (Haro-Corzo et al. 2007). AGNs were also suggested as nanodiamond factories (Rouan et al. 2004; Gratadour et al. 2006). Nanodiamonds efficiently form in UV and shocks (Jones & d’Hendecourt 2000). They could survive X-ray and UV radiation under conditions where silicate dust grains are destroyed.

1.4 Herbig Ae/Be stars

The infrared (IR) features at 3.43 and 3.53 μm in the spectra of the Herbig Ae/Be (HAeBe) stars Elias 1 (V892 Tau) and HD 97048 (CU Chamaeleontis) were explained by the C-H stretching vibrational modes in hydrogen-saturated diamonds present in protoplanetary disks (Guillois, Ledoux & Reynaud 1999; Jones & d’Hendecourt 2000; Van Kerckhoven, Tielens & Waelkens 2002; Habart et al. 2004; Topalović et al. 2006; Pirali et al. 2007; Goto et al. 2009). Majority of stars in the HAeBe class do not have spectral features at 3.43 and 3.53 μm (Acke & van den Ancker 2006). Elias 1 and HD 97048 were observed as sources of X-ray emission by several telescopes, for example in the ROSAT survey (Zinnecker & Preibisch 1994), by ASCA (Hamaguchi, Yamauchi & Koyama 2005), as well as by XMM-Newton and Chandra (Giardino et al. 2004; Skinner et al. 2004; Franciosini et al. 2007).

From IR observations it is known that 85% of HAeBe stars are binaries (Pirzkal, Spillar & Dyck 1997). It was proposed that nanodiamonds form in conditions where a protoplanetary disk exists around a hot star, with a companion emitting X-rays (Goto et al. 2009). Elias 1 is a triple star system in the Taurus-Auriga complex (Skinner, Brown & Stewart 1993; Leinert, Richichi & Haas 1997; Giardino et al. 2004; Smith et al. 2005; Franciosini et al. 2007). IR observations indicated that Elias 1 has a circumstellar disk of $\sim 0.1 M_{\odot}$ (Di Francesco et al. 1997). The first companion Elias 1 NE is in the T Tauri class, and it is located 4" north-east of Elias 1. The second companion was discovered by Smith et al. (2005). This convective star at 0.05", with mass of 1.5-2 M_{\odot} , was suggested as the source of X-rays. Giardino et al. (2004) found a strong X-ray flare in the triple Elias system. However, the presence of companions is not the only possible explanation of X-ray emission of HAeBe stars. For example, stellar winds and star-disk magnetospheres have been studied (Stelzer et al. 2006).

HD 97048 is a young star in the constellation Chamaeleon with a pronounced dusty disk (Habart et al. 2004; Doering et al. 2007). The dynamo model was proposed to explain X-ray emission in HD 97048 (Tout & Pringle 1995; Skinner et al. 2004). A protoplanetary disk with multiple rings and gaps around HD 97048 was recently observed (Ginski et al. 2016; Walsh et al. 2016; van der Plas et al. 2017).

1.5 Methane

Methane molecules are present in Earth’s atmosphere where they could interact with scattered solar and auroral X-rays. CH₄ was also observed in several extraterrestrial sources (Mousis et al. 2015). For example, the presence of methane was confirmed by Cassini spectrometers on the Saturn’s largest moon Titan (Niemann et al. 2005), as well as in the Enceladus plume (Waite et al. 2006). X-ray emission from Saturn was observed by XMM-Newton and Chandra (Branduardi-Raymont et al. 2010). CH₄ was detected in

comets (Gibb et al. 2003) and several comets were found to emit X-rays (Lisse et al. 1996; Dennerl, Englhauser & Trümper 1997; Lisse et al. 2001). Methane was also found in extrasolar planets (Swain, Vasisht & Tinetti 2008), the atmospheres of M-type stars (Jorgensen 1996), and the interstellar medium (Lacy et al. 1991). Kraus et al. (2017) recently performed the experiment on formation of diamonds in laser-compressed hydrocarbons. Conditions of this experiment simulated interiors of Neptune, Uranus and exoplanets. It is known that methane is very abundant in the atmospheres of Neptune, Uranus and some exoplanets. Methane transforms into a mixture of hydrocarbon polymers close to the surface of Uranus and Neptune. A phase separation into diamond and hydrogen is possible in deeper layers (Kraus et al. 2017). A transformation of CH₄ into diamond also occurs in the interior of icy super-earth mass planets (Levi et al. 2017).

1.6 Nanodiamonds

Surface atoms of nanodiamonds have unpaired bonds that are saturated with H atoms in a hydrogen rich atmosphere. The smallest nanodiamonds are adamantane (C₁₀H₁₆), diamantane (C₁₄H₂₀) and triamantane (C₁₈H₂₄). Isomers for higher nanodiamonds (starting from tetramantane C₂₂H₂₈) exist, and only some of them are tetrahedral. Oomens et al. (2006) studied IR spectra for several smaller nanodiamonds, from adamantane to hexamantane, and compared with astrophysical observations of V892 Tau and HD 97048. In addition, Pirali et al. (2007) extrapolated intensities of IR spectra of smaller nanodiamonds they studied. They found a good agreement between spectral intensities of larger tetrahedral diamondoids C₅₁H₅₂ and C₈₇H₇₆ and observed ones for Elias 1 and HD 97048. X-ray spectra of small nanodiamonds (up to hexamantane) were measured (Willey et al. 2005) but, to the best of our knowledge, similar studies on larger nanodiamonds do not exist. It is difficult to prepare large nanodiamonds on Earth by organic synthesis, or to extract them from petroleum. The largest tetrahedral nanodiamond discussed by Pirali et al. (2007), C₈₇H₇₆, is too large for available computational resources. Therefore, we calculate the K-edge X-ray spectrum of three tetrahedral hydrocarbon structures: CH₄, the [1(2,3)4] pentamantane isomer of C₂₆H₃₂, and C₅₁H₅₂. The nomenclature of isomers for diamondoids was introduced by Balaban & Von Rague Schleyer (1978).

Studies of X-ray spectra for materials in the astrophysical context are rather new, and till now done mainly for iron and silicate dust compounds using experimental synchrotron based methods (Lee & Ravel 2005; Lee et al. 2009; Zeegers et al. 2017; Rogantini et al. 2018). Calculations of scattering and absorption of X-rays (based on realistic dielectric functions) by carbonaceous and silicate dust grains are also available (Draine 2003). In this work density functional theory (DFT) is applied to calculate the X-ray absorption spectrum of tetrahedral hydrocarbon nanoparticles.

2 COMPUTATIONAL METHODS

DFT methods (Jones 2015), as implemented in the GPAW and ASE software suites (Enkovaara et al. 2010; Larsen et al. 2017), are used. DFT is a technique for modeling properties of quantum many-body systems by numerically calculating their electron density. We use DFT to study three tetrahedral hydrocarbon finite structures. The PBE generalized gradient approximation (GGA) (Perdew, Burke & Ernzerhof 1996) and the projector augmented wave method (PAW) (Blöchl 1994; Mortensen, Hansen & Jacobsen 2005) are applied.

The PAW method enables the reconstruction of the all-electron wave function and better modeling of X-ray spectra (Ljungberg, Mortensen & Pettersson 2011). The pseudopotential of the absorbing atom includes core-hole effects. The initial C 1s occupation is set to 0.5, in accordance with the transition potential approximation (Triguero, Pettersson & Ågren 1998). We have carried out half and full core calculations for all carbon atoms in all structures we study. The size of a computational box and the number of unoccupied states are investigated. Because of large sizes of nanodiamonds (in a comparison with simple molecules), we use the Haydock recursion method (Ljungberg, Mortensen & Pettersson 2011; Haydock, Heine & Kelly 1972) to calculate spectra and cover completely the post-edge region. The absolute energy scale is determined from the separate Delta Kohn-Sham calculations (Ljungberg, Mortensen & Pettersson 2011). Discrete transitions are broadened with Gaussians of the 0.5 eV width.

X-ray spectra we calculate show absorption of a sample as a function of energy. The energies of absorption edges are unique for each material sample and depend on its chemical composition, structure, electronic and vibrational properties. Spectral peak intensities in DFT studies of X-ray absorption are derived from the oscillator strengths which are dimensionless quantities (Stöhr 1996). As in other studies, we present the X-ray absorption intensity in arbitrary units. Although the exact values of dimensionless oscillator strengths are not important for comparison with experiments on Earth and observations of X-ray telescopes, it is appropriate to further develop theoretical methods to get the best values for these quantities. It is possible to compare the ratio of intensities for calculated oscillator strengths with the ratio of measured peaks. As an example, for hexamantane the ratio of the measured pre-edge peak intensity and the intensity of the K-edge is 0.8 (Willey et al. 2005). The same ratio we calculate for oscillator strengths is 0.4. This disagreement shows that DFT calculations are not quantitative enough to obtain oscillator strengths. However, energies of K and other edges are used to compare results with experiments in applications of X-ray absorption spectra. Good values for K-edges and overall agreement of our results and experimental spectra for methane (Hitchcock & Mancini 1994) and smaller nanodiamonds (Willey et al. 2005), as well as results for other systems calculated using the same methods (Triguero, Pettersson & Ågren 1998; Ljungberg, Mortensen & Pettersson 2011; Leetmaa et al. 2010; Susi et al. 2015; Sainio et al. 2016; LaRue et al. 2017) show that DFT methods we use are satisfactory. Other methods to calculate X-ray absorption spectra exist. Some of them are more rigorous than DFT, such as the many-body perturbation theory methods based on the Bethe-Salpeter equation (Shirley 1998; Rehr & Albers 2000; Gilmore et al. 2015). However, such methods are substantially more computationally demanding, especially for finite large structures we study in this work.

3 RESULTS AND DISCUSSION

3.1 X-ray spectra

The calculated carbon K-edge spectrum of methane is compared with the experimental result in Fig. 1. The corrected experimental electron energy-loss spectrum (EELS) from the database (Hitchcock & Mancini 1994) is used. The calculated (288.15 eV) and measured (288.12 eV) main peak differ by 0.01%. Methods we use do not produce a small pre-edge feature present in the EELS data. This feature is also absent in the spectrum of the gas phase

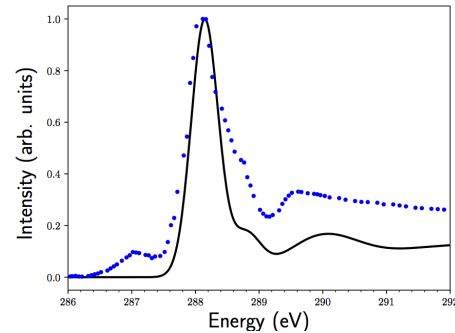


Figure 1. The X-ray spectra of methane. The dotted (blue) line is the experimental electron energy-loss result (Hitchcock & Mancini 1994). Full (black) line is the spectrum we calculate in this work.

CH₄ obtained by STOBED-DFT code (Öström et al. 2006). Such a small pre-edge peak appears in the high-resolution experimental spectra and the highest level *ab initio* theories because of a specific vibrational coupling effect on a dipole-forbidden transition (Schirmer et al. 1993).

The structures of C₂₆H₃₂ and C₅₁H₅₂ are shown in Fig. 2. Their X-ray spectra are presented in Figs. 3 and 4. The main broad peaks are positioned at 292 eV. Several smaller features appear from below of 287 eV up to the main peak. Pre-edge structures are more emphasized in the smaller nanodiamond C₂₆H₃₂. Similar pre-edge structures exist in experimental X-ray spectra of small nanodiamonds, from adamantane to hexamantane (Willey et al. 2005). These pre-edge features are contributions of the C-H and C-H₂ bonds at surfaces of nanodiamonds.

The internal structures of C₂₆H₃₂ and C₅₁H₅₂ resemble one of the bulk diamond (see Fig. 2). Features of the bulk diamond spectra for both C₂₆H₃₂ and C₅₁H₅₂ exist slightly below and at 305 eV (see Figs. 3 and 4). These bulk features are more pronounced for larger C₅₁H₅₂. However, spectra of large nanodiamonds C₂₆H₃₂ and C₅₁H₅₂ are still rather different from one of the bulk diamond. Our Figs. 3 and 4 are compared with measured (Ma et al. 1992) and calculated by the same GPAW methods (Ljungberg, Mortensen & Pettersson 2011) spectra of the bulk diamond. A different type of X-ray spectra of nanodiamonds we study and of the bulk diamond is in contrast to their optical spectra. It was measured that the optical response of the tetrahedral C₂₆H₃₂ isomer (shown in Fig. 2(a)) is similar to that of bulk diamond (Landt et al. 2009).

Many carbon species exhibit resonant spectral features in the 30 eV interval above the K-edge threshold of the carbon atom. The value of the K-edge for the carbon atom is 284 eV (Elam, Ravel & Sieber 2002). Examples are X-ray absorption spectra for benzene (C₆H₆) and cyclohexane (C₆H₁₂) condensed on the substrate, as well as the bulk diamond and graphite, shown together in Fig. 1.2 of the book by Stöhr (1996). It is obvious that pre-edge features do not exist for benzene, cyclohexane, bulk diamond and graphite. However, these pre-edge features are typical for spectra of nanodiamonds.

Bernatowicz, Gibbons & Lewis (1990) measured the EELS spectrum of the carbonaceous meteorites Murray and Allende. Their presented spectrum for the Murray meteorite approximately resembles our result. However, pre-edge features are more pronounced in our Figs. 3 and 4. This shows that hydrogenated nanodiamonds are only one of components in the Murray meteorite. Nanodiamonds in the Allende and Murchison meteorites were ana-

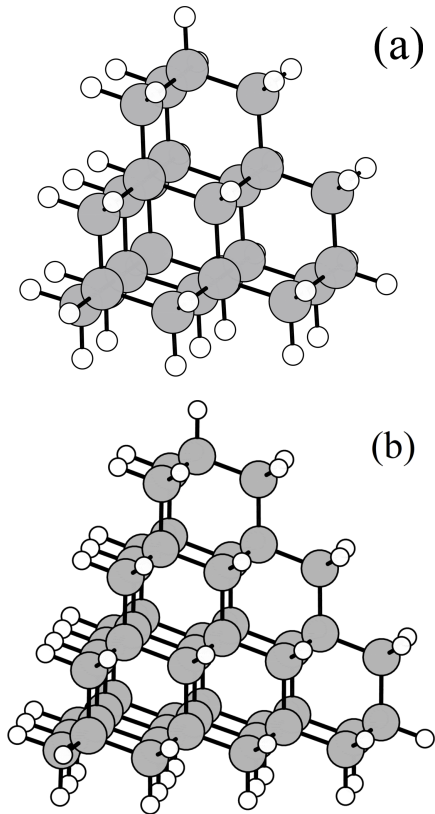


Figure 2. The optimized structures of: (a) $C_{26}H_{32}$, (b) $C_{51}H_{52}$. Darker larger balls represent carbon and lighter smaller balls hydrogen atoms.

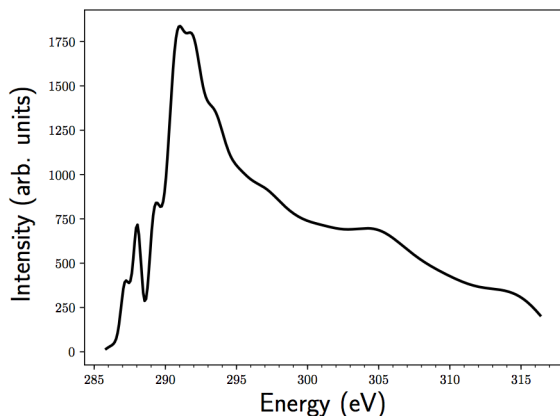


Figure 3. The X-ray absorption spectrum of $C_{26}H_{32}$.

lyzed by Stroud et al. (2011). They concluded that these meteorites consist of a two-phase mixture of nanodiamonds and glassy carbon. Stroud et al. (2011) proposed that this complex material is the product of supernova shock-waves. The presence of glassy carbon changes the EELS spectrum of meteorites. Therefore, Stroud et al. (2011) separately measured EELS spectra from nanodiamonds and glassy carbon regions. The spectrum of regions with nanodiamonds is similar to the spectra shown in Figs. 3 and 4.

CO is the second most abundant molecule in the ISM. Its carbon K-edge is at 287.4 eV (Hitchcock & Mancini 1994), and it is positioned in the pre-edge region of nanodiamonds. Pre-edge

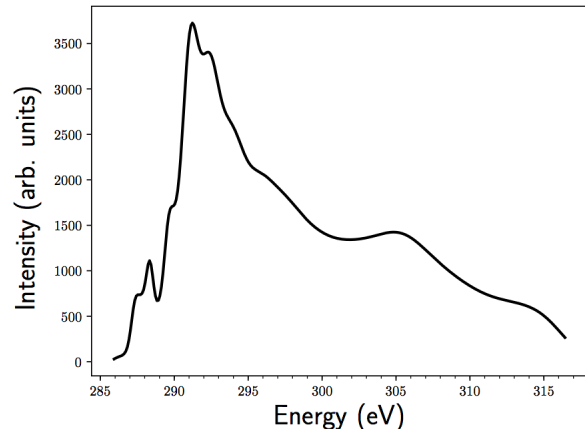


Figure 4. The X-ray absorption spectrum of $C_{51}H_{52}$.

Structure	a_{max} (Å)
$C_{26}H_{32}$	7.3
$C_{51}H_{52}$	9.7
$C_{87}H_{76}$	11.6
$C_{136}H_{104}$	14.7
bucky diamonds	20-30

Table 1. DFT optimized morphologies and sizes of several diamond related carbon nanoparticles. Four large tetrahedral nanodiamonds are shown, as well as bucky diamonds. It was found that bucky diamonds are more stable in the size region shown in Table 1, for a broad range of pressures and temperatures (Raty & Galli 2003; Galli 2010). The a_{max} values show the maximum of distances between atoms in a corresponding structure.

features of nanodiamonds have smaller intensities in a comparison with the carbon K-edge of the CO molecule. In addition, the carbon K-edge of CO is linked with its oxygen K-edge at 534.2 eV (Hitchcock & Mancini 1994). There are no features in X-ray spectra of nanodiamonds at > 500 eV. Therefore, CO does not prevent a detection of nanodiamonds from their X-ray spectra. X-ray spectra of other carbon and carbon-hydrogen species in space (for example PAHs) are not similar to the spectra of nanodiamonds. These other carbon compounds do not have a pre-edge region. X-ray spectra of nanodiamonds are specific, with its pre-edge, edge, and post-edge regions.

In previous DFT calculations it was found that bucky diamonds are more stable than nanodiamonds for sizes (2-3) nm, and for a broad range of temperatures and pressures (Raty & Galli 2003; Galli 2010). Bucky diamonds consist of a diamond core and a fullerene-like surface layers with a mixed pentagon-hexagon network. Hydrogen atoms are absent. Sizes of tetrahedral nanodiamonds and bucky diamonds are compared in Table 1. It is interesting that fullerenes are also discovered in space (Tielens 2013). Therefore, several diamond related nanoparticles should be considered in astrochemistry. X-ray spectra of nanodiamonds (Figs. 3 and 4), as well as Table 1, show that fitting of dust properties to the bulk diamond values (i.e. those measured for a diamond cubic lattice) could produce errors. Nanodiamonds or bucky diamonds could be more stable for some conditions in space.

A recent comparison of *Swift* X-ray/FUV observations with those done using *ALMA* radio telescope for the T Tauri star IM Lup pointed out the importance of X-ray flare-driven chemistry in the circumstellar disk (Cleeves et al. 2017). Flare-driven processes could be also present at Elias 1 and HD 97048. A strong flare in the Elias triple system was already observed by Giardino et al. (2004). Flares could induce the formation of nanodiamonds from amorphous and graphitic-like dust grains, as well as destroy smallest diamond nanoparticles in protoplanetary disks. Bigger ones such as $C_{51}H_{52}$ should remain. This agrees with studies of IR spectra by Pirali et al. (2007) where it was found that measured spectral intensities of large nanodiamonds correspond to astronomical observations of Elias 1 and HD 97048.

3.2 Detection of nanodiamonds by X-ray telescopes

We propose a detection of large tetrahedral nanodiamonds by future high-resolution X-ray telescopes such as *Arcus* (Smith et al. 2016; Brennen et al. 2016). *Arcus* is the soft X-ray grating spectrometer project submitted to NASA in 2016. It was selected for a Phase A concept study in August 2017. *Arcus* should work with an effective area $>500 \text{ cm}^2$, spectral resolution $R=\lambda/\Delta\lambda >4000$, and in the (8-51) Å (i.e., (0.24-1.55) keV) range. *Arcus* will study sources in the Milky Way and other galaxies. Science questions which *Arcus* should answer are broad and range from baryons in the Universe, black holes, galaxy clusters and the cosmic web, to various stars, their protoplanetary disks and exoplanets. When its baseline missions will be completed, *Arcus* will study additional scientific questions. We suggest that properties of nanodiamonds and other forms of carbon dust should be studied, as *Arcus* will be capable of discriminating between them, as well as between different types of diamond nanoparticles (see Fig. 5). Till now X-ray spectral studies of cosmic dust were focused on iron and silicate based grains (Lee & Ravel 2005; Lee et al. 2009; Zeegers et al. 2017; Rogantini et al. 2018). However, carbon astrochemistry is very rich and important to understand various processes in the evolution of galaxies, stars and planets.

For the target sources we propose to look at HAeBe stars Elias 1 (V892 Tau) and HD 97048 (CU Chamaeleontis) where the existence of nanodiamonds was confirmed by IR spectroscopy (Guillois, Ledoux & Reynaud 1999; Jones & d’Hendecourt 2000; Van Kerckhoven, Tielens & Waelkens 2002; Habart et al. 2004; Topalović et al. 2006; Pirali et al. 2007; Goto et al. 2009). These stars are also confirmed as X-ray sources by previous generations of X-ray telescopes (Zinnecker & Preibisch 1994; Hamaguchi, Yamauchi & Koyama 2005; Giardino et al. 2004; Skinner et al. 2004; Franciosini et al. 2007). Additional target sources are supernovae (Tielens et al. 1987) and active galactic nuclei (Haro-Corzo et al. 2007; Rouan et al. 2004; Gratadour et al. 2006).

Further, a target source need not be previously identified as rich in nanodiamonds; the diffuse ISM itself may harbor them in small quantities such as 5% (Tielens et al. 1987), though possibly as high as 10% (Lewis, Anders & Draine 1989). To examine this, we have simulated an *Arcus* spectrum of Cyg X-2 (see Fig. 5) using the fit of the source’s Chandra/ACIS spectrum by Seward & Smith (2013). We modeled it as an absorbed disk blackbody, with $N_H=1.7 \times 10^{21} \text{ cm}^{-2}$, $T_{in}=1.5 \text{ keV}$, and $F_X(0.25 - 1.25 \text{ keV})=1.4 \times 10^{-9} \text{ erg cm}^{-2} \text{ s}^{-1}$. We assumed the proto-solar elemental abundances of Lodders (2003). Following Kaastra, Mewe & Nieuwenhuijzen (1996) and Pinto et al. (2010), we then estimated the nanodiamond cross sections by scaling them to the free atom photoionization cross sections of Verner & Yakovlev (1995). The

scaled cross sections were then merged with the free atom cross sections, so that the scaled cross sections would be used over their energy range, and the free atom cross sections would be used outside that range. Léger et al. (1991) found that PAHs account for 10% of the carbon in the ISM. To approximate the PAHs contribution, we obtained the experimental EELS of benzene (C_6H_6) from the online database (Hitchcock & Mancini 1994) and scaled it in the same way as the nanodiamond spectra. We then made a series of simulated spectra, setting quantities of C_6H_6 and carbon gas to 10% and 80% of total available carbon, respectively, with the remaining 10% in nanodiamonds. We fitted the spectra from (280-330) eV and allowed all parameters to float. An implementation of the Cash statistic, *cstat*, was used to find the best fits (Cash 1976; Arnaud, Smith & Siemiginowska 2011). When the nanodiamond contribution was set to be either entirely $C_{26}H_{32}$ or $C_{51}H_{52}$, they could be detected to 5σ in 200 ks. Next, we tested to see if we could distinguish between diamond types by fitting the spectrum with all $C_{26}H_{32}$ absorption with a model using $C_{51}H_{52}$. This produced a goodness-of-fit value (*cstat/degrees of freedom*) of 2660/2607. For comparison, the value obtained from fitting it with a model using $C_{26}H_{32}$ was 2643/2607, indicating that the nanodiamond types can be distinguished. Similar results were obtained when testing the spectrum with all $C_{51}H_{52}$ absorption in the same way. The simulated spectra with all $C_{26}H_{32}$ and all $C_{51}H_{52}$ nanodiamonds are shown in the top and middle panels of Fig.5, respectively. We also considered the case where $C_{26}H_{32}$ and $C_{51}H_{52}$ each accounted for 5% of the total C available. The exposure time required for 5σ detections of both diamond types rose to 4 Ms (see Fig.5, bottom panel). While this is a large time investment, determining the nanodiamond size distribution in the diffuse ISM could shed light on diamond formation and destruction (Tielens et al. 1987). Further, both the oxygen K and iron L edges fall within the *Arcus* bandpass, and such an observation would allow an examination of silicate and iron-bearing dust features in unprecedented detail at those edges, as well.

4 CONCLUSIONS

Nanodiamonds have been a subject of research in astrophysics for a long time. They have been involved in diverse topics such as Earth and planetary astrophysics, the interstellar medium, stars, supernovae, pulsars, and active galactic nuclei. However, nanodiamonds are still rather unexplored type of cosmic dust. We calculate the X-ray absorption spectra at the carbon K-edge of tetrahedral hydrocarbon nanoparticles CH_4 , $C_{26}H_{32}$, and $C_{51}H_{52}$ using density functional theory methods. A specific combination of pre-edge, edge, and post-edge features differs from spectra of other carbon and C-H species and could be used for detection of nanodiamonds by X-ray spectroscopy. We suggest detection studies of nanodiamonds (as well as other forms of carbon based cosmic dust) by future X-ray telescopes, such as the project *Arcus* recently selected by NASA for a Phase A concept study. In particular, active galactic nuclei are favorable environments for the formation of nanodiamonds. Diamond nanoparticles efficiently form in UV shocks and they could survive harsh environments where silicate dust is destroyed. Strong target candidates to detect nanodiamonds by X-ray spectroscopy are X-ray active Herbig Ae/Be stars Elias 1 (V892 Tau) and HD 97048 (CU Chamaeleontis).

The results of DFT calculations can be scaled and used in ISM spectral fitting. Here, to simulated *Arcus* spectra we have applied the method that was used to scale similar molecular spec-

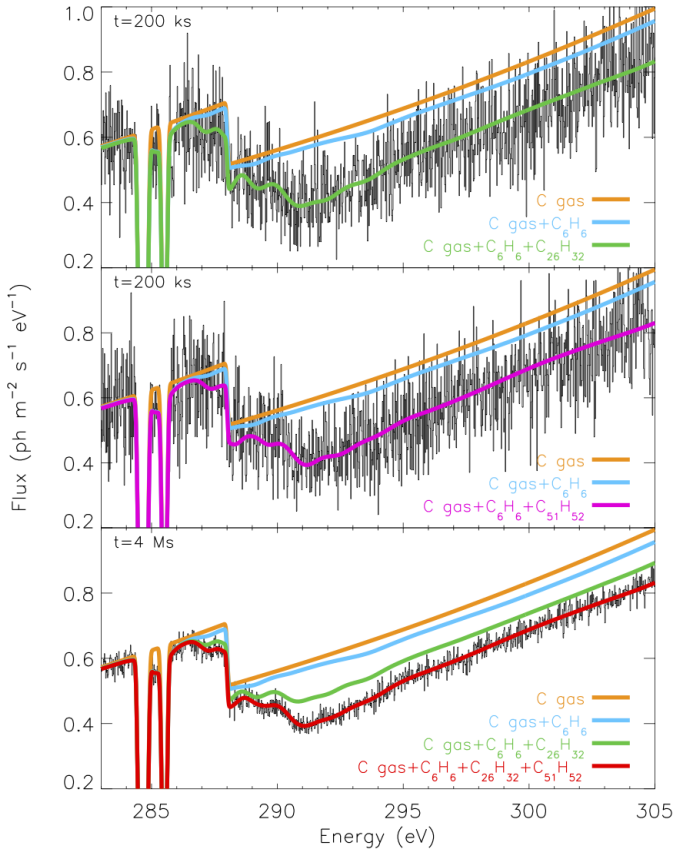


Figure 5. Simulated *Arcus* spectra of Cyg X-2 at the carbon K edge, for different exposure times, as well as nanodiamond types and amounts.

tra (i.e., spectra in arbitrary flux units). Using the scaled spectra, we have simulated an observation of absorption in the diffuse ISM ($N_H=10^{21} \text{ cm}^{-2}$) toward a bright source (Cyg X-2), using standard values for ISM carbon abundance. We have set the amounts of carbon in diamonds and PAHs each to 10%, respectively, as suggested by the literature; when only one type of diamond was used, the absorption from nanodiamonds could be detected to 5σ and the diamond type could be distinguished in a 200 ks observation.

ACKNOWLEDGEMENTS

Calculations presented in this work were done using the computational cluster Isabella at the University of Zagreb Computing Centre SRCE. GB acknowledges the support of the Croatian Science Foundation (HRZZ) grant IP-2014-09-8656. We would like to thank Elisa Costantini and Sascha Zeegers for discussions. We thank the referee for useful suggestions. This research has made use of NASA's Astrophysics Data System Bibliographic Services.

REFERENCES

- Acke B., van den Ancker M. E., 2006, *A&A*, 457, 171
- Arnaud K., Smith R., Siemiginowska A., 2011, *Handbook of X-ray Astronomy*. Springer
- Bailes M. et al., 2011, *Science*, 333, 1717
- Balaban A. T., Von Rague Schleyer P., 1978, *Tetrahedron*, 34, 3599
- Bernatowicz T. J., Gibbons P. C., Lewis R. S., 1990, *ApJ*, 359, 246
- Blöchl P. E., 1994, *Phys. Rev. B*, 50, 17953
- Branduardi-Raymont G., Bhardwaj A., Elsner R. F., Rodriguez P., 2010, *A&A*, 510, A73
- Brenneman L. W. et al., 2016, in *Proc. SPIE, Vol. 9905, Space Telescopes and Instrumentation 2016: Ultraviolet to Gamma Ray*, p. 99054P
- Cash W., 1976, *A&A*, 52, 307
- Chang H. C., Chen K., Kwok S., 2006, *ApJ*, 639, L63
- Clay W. A., Dahl J. E. P., Carlson R. M. K., Melosh N. A., Shen Z.-X., 2015, *Rep. Prog. Phys.*, 78, 016501
- Cleeves L. I., Bergin E. A., Öberg K. I., Andrews S. M., Wilner D. J., Loomis R. A., 2017, *ApJL*, 843, L3
- Dai Z. R., Bradley J. P., Joswiak D. J., Brownlee D. E., Hill H. G. M., Genge M. J., 2002, *Nature*, 418, 157
- Daulton T., Eisenhour D., Bernatowicz T., Lewis R., Buseck P., 1996, *Geochim. Cosmochim. Acta*, 60, 4853
- Dennerl K., Englhauser J., Trümper J., 1997, *Science*, 277, 1625
- Di Francesco J., Evans, II N. J., Harvey P. M., Mundy L. G., Guilleloteau S., Chandler C. J., 1997, *ApJ*, 482, 433
- Doering R. L., Meixner M., Holfeltz S. T., Krist J. E., Ardila D. R., Kamp I., Clampin M. C., Lubow S. H., 2007, *AJ*, 133, 2122
- Draine B. T., 2003, *ApJ*, 598, 1026
- Duley W. W., 1988, *ApSS*, 150, 387
- Elam W., Ravel B., Sieber J., 2002, *Radiat. Phys. Chem.*, 63, 121, available online at <http://xafs.org/Databases/XrayTable>
- Enkovaara J. et al., 2010, *J. Phys.: Cond. Matt.*, 22, 253202
- Franciosi E. et al., 2007, *A&A*, 468, 485
- Galli G., 2010, in *Computer-Based Modeling of Novel Carbon Systems and Their Properties*, Colombo L., Fasolino A., eds., Springer, Berlin, pp. 37–56
- Geballe T. R., Noll K. S., Whittet D. C. B., Waters L. B. F. M., 1989, *ApJL*, 340, L29
- Giardino G., Favata F., Micela G., Reale F., 2004, *A&A*, 413, 669
- Gibb E., Mumma M., Russo N. D., DiSanti M., Magee-Sauer K., 2003, *Icarus*, 165, 391
- Gilmore K., Vinson J., Shirley E., Prendergast D., Pemmaraju C., Kas J., Vila F., Rehr J., 2015, *Comput. Phys. Commun.*, 197, 109
- Ginski C. et al., 2016, *A&A*, 595, A112
- Goto M. et al., 2009, *ApJ*, 693, 610
- Gratadour D., Rouan D., Mugnier L. M., Fusco T., Clénet Y., Gendron E., Lacombe F., 2006, *A&A*, 446, 813
- Guillois O., Ledoux G., Reynaud C., 1999, *ApJ*, 521, L133
- Habart E., Testi L., Natta A., Carbillet M., 2004, *ApJ*, 614, L129
- Hamaguchi K., Yamauchi S., Koyama K., 2005, *ApJ*, 618, 360
- Haro-Corzo S. A. R., Binette L., Krongold Y., Benitez E., Humphrey A., Nicastro F., Rodríguez-Martínez M., 2007, *ApJ*, 662, 145
- Haydock R., Heine V., Kelly M. J., 1972, *J. Phys. C: Solid State Phys.*, 5, 2845
- Helling C., Tootill D., Woitke P., Lee G., 2017, *A&A*, 603, A123
- Hitchcock A. P., Mancini D. C., 1994, *J. Electron Spectrosc. Relat. Phenom.*, 67, 1, available online at <http://unicorn.mcmaster.ca/corex/Search-List.html>
- Jones A. P., d'Hendecourt L., 2000, *A&A*, 355, 1191
- Jones R. O., 2015, *Rev. Mod. Phys.*, 87, 897
- Jorgensen U. G., 1996, in *IAU Symposium, Vol. 178, Molecules in Astrophysics: Probes & Processes*, van Dishoeck E. F., ed., p. 441
- Kaastra J. S., Mewe R., Nieuwenhuijzen H., 1996, in *UV and X-*

- ray Spectroscopy of Astrophysical and Laboratory Plasmas, Yamashita K., Watanabe T., eds., pp. 411–414
- Kennett D. J. et al., 2009, *Science*, 323, 94
- Kraus D. et al., 2017, *Nat. Astron.*, 1, 606
- Kuchner M. J., Seager S., 2005, *astro-ph/0504214*
- Lacy J. H., Carr J. S., Evans, II N. J., Baas F., Achtermann J. M., Arens J. F., 1991, *ApJ*, 376, 556
- Landt L., Klünder K., Dahl J. E., Carlson R. E. E. K., Möller T., Bostedt C., 2009, *Phys. Rev. Lett.*, 103, 047402
- Larsen A. H. et al., 2017, *J. Phys.: Cond. Mat.*, 29, 273002
- LaRue J. et al., 2017, *J. Phys. Chem. Lett.*, 8, 3820
- Lee J. C., Ravel B., 2005, *ApJ*, 622, 970
- Lee J. C., Xiang J., Ravel B., Kortright J., Flanagan K., 2009, *ApJ*, 702, 970
- Leetmaa M., Ljungberg M., Lyubartsev A., Nilsson A., Pettersson L., 2010, *J. Electron Spectrosc. Relat. Phenom.*, 177, 135
- Léger A., D’Hendecourt L., Verstraete L., Joblin C., 1991, in *Lecture Notes in Physics*, Berlin Springer Verlag, Vol. 390, *Bioastronomy: The Search for Extraterrestrial Life - The Exploration Broadens*, Heidmann J., Klein M. J., eds., pp. 88–92
- Leinert C., Richichi A., Haas M., 1997, *A&A*, 318, 472
- Levi A., Kenyon S. J., Podolak M., Prialnik D., 2017, *ApJ*, 839, 111
- Lewis R. S., Anders E., Draine B. T., 1989, *Nature*, 339, 117
- Lewis R. S., Ming T., Wacker J. F., Anders E., Steel E., 1987, *Nature*, 326, 160
- Lisse C. M., Christian D. J., Dennerl K., Meech K. J., Petre R., Weaver H. A., Wolk S. J., 2001, *Science*, 292, 1343
- Lisse C. M. et al., 1996, *Science*, 274, 205
- Ljungberg M. P., Mortensen J. J., Pettersson L. G. M., 2011, *J. Electron Spectrosc. Relat. Phenom.*, 184, 427
- Lodders K., 2003, *ApJ*, 591, 1220
- Ma Y. et al., 1992, *Phys. Rev. Lett.*, 69, 2598
- Margalit B., Metzger B. D., 2017, *MNRAS*, 465, 2790
- Mortensen J. J., Hansen L. B., Jacobsen K. W., 2005, *Phys. Rev. B*, 71, 035109
- Mousis O. et al., 2015, *Astrobiology*, 15, 308
- Niemann H. B. et al., 2005, *Nature*, 438, 779
- Oomens J. et al., 2006, *J. Mol. Spectrosc.*, 238, 158
- Öström H., Ogasawara H., Näslund L.-A., Pettersson L. G. M., Nilsson A., 2006, *Phys. Rev. Lett.*, 96, 146104
- Perdew J. P., Burke K., Ernzerhof M., 1996, *Phys. Rev. Lett.*, 77, 3865
- Pinto C., Kaastra J. S., Costantini E., Verbunt F., 2010, *A&A*, 521, A79
- Pirali O., Vervloet M., Dahl J. E., Carlson R. M. K., Tielens A. G. G. M., Oomens J., 2007, *ApJ*, 661, 919
- Pirzkal N., Spillar E. J., Dyck H. M., 1997, *ApJ*, 481, 392
- Rai R. K., Rastogi S., 2012, *MNRAS*, 423, 2941
- Raty J., Galli G., 2003, *Nature Mat.*, 2, 792
- Rehr J. J., Albers R. C., 2000, *Rev. Mod. Phys.*, 72, 621
- Rogantini D., Costantini E., Zeegers S. T., de Vries C. P., Bras W., de Groot F., Mutschke H., Waters L. B. F. M., 2018, *A&A*, 609, A22
- Rouan D. et al., 2004, *A&A*, 417, L1
- Sainio S. et al., 2016, *J. Phys. Chem. C*, 120, 8298
- Saslaw W. C., Gaustad J. E., 1969, *Nature*, 221, 160
- Schirmer J., Trofimov A. B., Randall K. J., Feldhaus J., Bradshaw A. M., Ma Y., Chen C. T., Sette F., 1993, *Phys. Rev. A*, 47, 1136
- Seward F. D., Smith R. K., 2013, *ApJ*, 769, 17
- Shirley E. L., 1998, *Phys. Rev. Lett.*, 80, 794
- Skinner S. L., Brown A., Stewart R. T., 1993, *ApJS*, 87, 217
- Skinner S. L., Güdel M., Audard M., Smith K., 2004, *ApJ*, 614, 221
- Smith K. W., Balega Y. Y., Duschl W. J., Hofmann K.-H., Lachaume R., Preibisch T., Schertl D., Weigelt G., 2005, *A&A*, 431, 307
- Smith R. K. et al., 2016, in *Proc. SPIE*, Vol. 9905, *Space Telescopes and Instrumentation 2016: Ultraviolet to Gamma Ray*, p. 99054M
- Stelzer B., Micela G., Hamaguchi K., Schmitt J. H. M. M., 2006, *A&A*, 457, 223
- Stöhr J., 1996, *NEXAFS Spectroscopy*. Springer
- Stroud R. M., Chisholm M. F., Heck P. R., Alexander C. M. O., Nittler L. R., 2011, *ApJL*, 738, L27
- Susi T., Mowbray D. J., Ljungberg M. P., Ayala P., 2015, *Phys. Rev. B*, 91, 081401
- Swain M. R., Vasisht G., Tinetti G., 2008, *Nature*, 452, 329
- Tielens A. G. G. M., 2013, *Rev. Mod. Phys.*, 85, 1021
- Tielens A. G. G. M., Seab C. G., Hollenbach D. J., McKee C. F., 1987, *ApJ*, 319, L109
- Topalović R., Russell J., McCombie J., Kerr T. H., Sarre P. J., 2006, *MNRAS*, 372, 1299
- Tout C. A., Pringle J. E., 1995, *MNRAS*, 272, 528
- Triguero L., Pettersson L. G. M., Ågren H., 1998, *Phys. Rev. B*, 58, 8097
- van der Plas G. et al., 2017, *A&A*, 597, A32
- Van Kerckhoven C., Tielens A. G. G. M., Waelkens C., 2002, *A&A*, 384, 568
- Verner D. A., Yakovlev D. G., 1995, *A&AS*, 109, 125
- Waite J. H. et al., 2006, *Science*, 311, 1419
- Walsh C., Juhász A., Meeus G., Dent W. R. F., Maud L. T., Aikawa Y., Millar T. J., Nomura H., 2016, *ApJ*, 831, 200
- Wentorf, Jr. R. H., Bovenkerk H. P., 1961, *ApJ*, 134, 995
- Willey T. M., Bostedt C., van Buuren T., Dahl J. E., Liu S. G., Carlson R. M. K., Terminello L. J., Möller T., 2005, *Phys. Rev. Lett.*, 95, 113401
- Zeegers S. T. et al., 2017, *A&A*, A117
- Zinnecker H., Preibisch T., 1994, *A&A*, 292, 152